Check for updates

A double helix of opposite charges to form channels with unique CO_2 selectivity and dynamics†

Guolong Xing, [ID] [a] Irene Bassanetti, [ID] [b] Silvia Bracco, [ID] [b] Mattia Negroni, [ID] [b] Charl Bezuidenhout, [ID] [b] Teng Ben, [ID] *[a] Piero Sozzani [ID] *[b] and Angiolina Comotti [ID] *[b]

Porous molecular materials represent a new front in the endeavor to achieve high-performance sorptive properties and gas transport. Self-assembly of polyfunctional molecules containing multiple charges, namely, tetrahedral tetra-sulfonate anions and bifunctional linear cations, resulted in a permanently porous crystalline material exhibiting tailored sub-nanometer channels with double helices of electrostatic charges that governed the association and transport of CO_2 molecules. The charged channels were consolidated by robust hydrogen bonds. Guest recognition by electrostatic interactions remind us of the role played by the dipolar helical channels in regulatory biological membranes. The systematic electrostatic sites provided the perfectly fitting *loci* of complementary charges in the channels that proved to be extremely selective with respect to N_2 ($S = 690$), a benchmark in the field of porous molecular materials. The unique screwing dynamics of CO_2 travelling along the ultramicropores with a step-wise reorientation mechanism was driven by specific host–guest interactions encountered along the helical track. The unusual dynamics with a single-file transport rate of more than 10^6 steps per second and an energy barrier for the jump to the next site as low as 2.9 kcal mol^{-1} was revealed unconventionally by complementing *in situ* ^{13}C NMR anisotropic line-shape analysis with DFT modelling of CO_2 diffusing in the crystal channels. The peculiar sorption performances and the extraordinary thermal stability up to 450 °C, combined with the ease of preparation and regeneration, highlight the perspective of applying these materials for selective removal of CO_2 from other gases.

Introduction

The manufacture of materials with permanent porosity is one of the major challenges in current research. This goal can be achieved through various strategies that promote the formation of covalent and metal–organic frameworks as well as molecular architectures.[1–8] They are diversified by their greater or lesser tendency to form stable structures and their degree of crystalline periodicity. Highly crystalline porous molecular materials can be constructed easily by spontaneous assembly of precursor molecules, provided that their shapes and functionalities are adequately designed.[9–11] Indeed, fully organic porous materials can be assembled by means of soft and reversible interactions enabling the highest modularity, processability and large

single-crystal formation. Their excellent performances in gas capture and interaction with chemical and physical stimuli have been explored in recent years.[12–29]

Organic functions of opposite charges on complementary molecules promote intense attractive interactions, and reciprocal recognition such as positively charged ammonium groups with carboxylic and sulfonic anions; thus, electrostatic interactions can be exploited to sustain robust molecular frameworks.[30–35] Additionally, electrostatic charges can be exposed to the pores, making it possible to expand research towards unexplored developments.

In our approach, multiple-charged functional groups protruding in the space produce directional interactions, favourable to the design of porous molecular architectures, forming programmable charged channels. In general, the shape and symmetry of the building blocks to construct porous frameworks must be taken into account: specifically, highly symmetric and rigid tetrahedral struts (S_4 point group) constitute a primary element, which sustained permanently porous materials and yielded very high surface areas.[36–44]

Biological systems are promising sources for the formation of sub-nanometer channels for the transport of molecules and

[a]Department of Chemistry, Jilin University, Changchun 130012, People's Republic of China

[b]Department of Materials Science, University of Milano Bicocca, Via R. Cozzi 55, Milan, Italy. E-mail: angiolina.comotti@unimib.it

† Electronic supplementary information (ESI) available. CCDC 1865475 and 1865476. For ESI and crystallographic data in CIF or other electronic format see DOI: 10.1039/c8sc04376k

ions, wherein the electrostatic distribution of charges on the channel walls and steric factors play a strategic role for building useful functions.[45] By analogy, we have engineered a permanently porous 3D molecular architecture containing sub-nm channels formed by a double helix with two intertwined and alternatively charged ribbons, characteristic of transmembrane channels. It was generated by the assembly of tetrahedral and tetrafunctional 4,4′,4″,4‴-methane tetrabenzenesulfonate (TBS) anions and a bifunctional cation 1,4-diamidiniumbenzene (DAB) and was found to be highly stable. The porous structure was capable of reversibly absorbing relevant gases such as CO_2 and CH_4 with an exceptional CO_2/N_2 selectivity of 690 owing to the tight fitting and the complementary electrostatic pattern of the sub-nm channels. The direct detection of CO_2 pervading the porous molecular framework was provided by multinuclear 2D MAS NMR spectra, depicting the exceptional CO_2-matrix association in the properly fitting pockets. Furthermore, the anisotropic ^{13}C NMR variable-temperature lineshapes unveiled the unique coordinated rotation and translation dynamics of CO_2 while it jumps from one site to the next, following the helical charge patterning of the channel. Intriguingly, CO_2 molecules receive the orientational encoding from the nanochannel sites at each diffusion turn of the screwing motion. Thus, by this unconventional means, we could establish the transport rate of a single gas molecule that is as fast as a million steps per second, corresponding to guest diffusion rates observed in biological channels. DFT calculations and Molecular Dynamics (MD) supported the NMR determination of the preferred arrangement and the energy landscape perceived by CO_2 exploring the channels.

Results and discussion

Fabrication of charged sub-nanometer channels

The organotetrasulfonate TBS self-assembled with organo-diamidinium DAB to form needlelike single crystals suitable for X-ray analysis (ESI†). After guest removal by thermal treatment under vacuum at 150 °C, the 3D architecture is maintained, yielding a new crystalline porous organosulfonate–amidinium salt (CPOS-5) (Fig. 1). It crystallizes in the tetragonal $I4_1a$ space group, which contains a quarter of TBS (a phenyl-SO_3^- group) and half of DAB in the asymmetric unit (molecular formula equal to TBS(DAB)$_2$). A 4-fold rotoinversion axis crosses the central carbon (C1), which orients four sulphonate groups along the vertices of a tetrahedron. Hence, organosulfonate anions and organoamidinium cations, driven by hydrogen bonds,

Fig. 1 (A) Schematic representation of anionic TBS and cationic DAB synthons of the porous organic framework. (B) View of the porous framework along the c-axis; yellow represents the empty channels (a rolling sphere of 1.4 Å was used). The channel running parallel to the c-axis: (C) the synthons are connected through a H-bonding network in a helical fashion; (D) electrostatic map showing the positively and negatively charged helical ribbons.
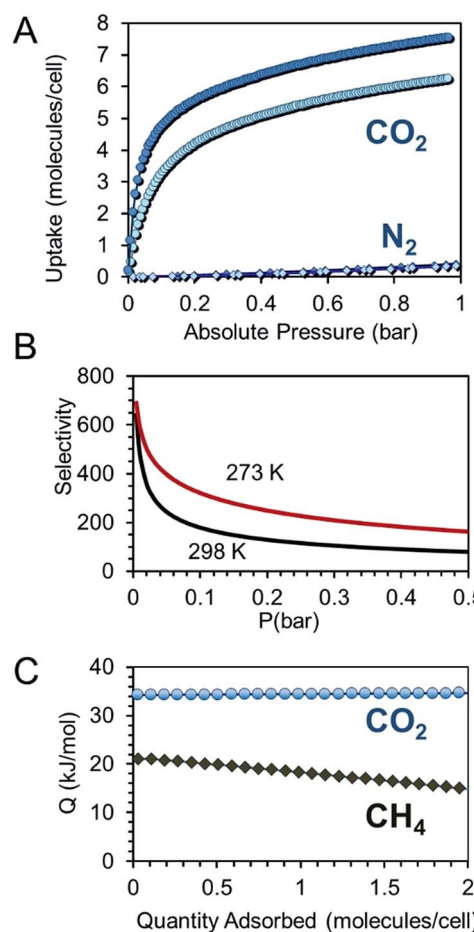

Fig. 2 (A) CO_2 and N_2 isotherms of CPOS-5 collected at 273 K (blue circles and diamonds, respectively) and 298 K (light-blue circles and diamonds, respectively). (B) CO_2/N_2 selectivity values of CPOS-5 versus pressure calculated starting from a 15/85 mixture and applying IAST calculation. (C) Isosteric heats of adsorption (Q_{st}) versus CO_2 and CH_4 loading.

assemble in a double helix of electrically charged ribbons (Fig. 1C). Both negatively and positively charged moieties draw alternatively charged helices that lead to the formation of 1D-channels (Fig. 1D), running parallel to the c-axis. The empty channels with a cross-section of 5.3×6.8 Å^2 generate a porosity of 743.03 Å^3 per cell corresponding to 14.6% of the cell volume (radius of the rolling sphere = 1.2 Å). The ^{13}C MAS NMR spectrum confirmed the absence of guests in the cavities (ESI†). The porous compound exhibits high stability to water and temperature (up to 400 °C) owing to the connection of four organosulfonate anions to DAB monomers through charge-assisted hydrogen bonds in all directions.

Gas capture and CO$_2$ selectivity

CO$_2$ adsorption isotherms were collected on CPOS-5 to demonstrate its permanent porosity (Fig. 2). Interestingly, at 273 K the CO$_2$ adsorption isotherm displayed a Langmuir profile, which at 1 bar reached the value of 48 cm^3 g^{-1}, representing 8 CO$_2$ molecules per unit cell (Fig. 2A). Notably, CO$_2$ uptake was already extremely high at low pressure and exhibited a loading as high as 59 mg g^{-1} (273 K) at 0.1 bar, suggesting excellent affinity of the quadrupolar gas molecules with charge-decorated pore

surfaces. At 0.1 bar and at room temperature, typical conditions of CO$_2$ pressure in flue gas from power plants, CPOS-5 adsorbs 39 mg g^{-1}, outperforming many well-known MOFs with greater surface areas such as HKUST-1, UMCM-150(N2), MIL-47, IRMOF-3 and ZIF-8,[46] porous hydrogen-bonds and supramolecular organic frameworks such as SOF-1,[23] SOF-7,[47] HOF-3 (ref. 27) and CB6 (ref. 17) and its absorption value is comparable to that of the best performing HOF-5.[24]

The isosteric heat of adsorption Q_{st} calculated using the van't Hoff equation accounted for 34.5 kJ mol^{-1}, which is in agreement with the binding energy determined by DFT calculations $\Delta E = 33.8$ kJ mol^{-1} (ESI†). The Q_{st} value is comparable to those of some high-performance porous crystalline materials such as SOF-1,[23] MIL-53,[48] HKUST-1 (ref. 49) and NaX zeolites,[50] which contain channels decorated with charged moieties.

The prominent difference in the CO$_2$ uptake with respect to N$_2$ under the same pressure and temperature conditions prompted us to calculate the CO$_2$/N$_2$ selectivity using Ideal Adsorbed Solution Theory (IAST) applied to single-component isotherms starting from a 15 : 85 (CO$_2$: N$_2$) mixture in order to simulate the flue gas conditions (Fig. 2B). The CO$_2$/N$_2$ selectivity at 273 K exhibited values in the 320–690 range at low

Fig. 3 CPOS-5 loaded with ^{13}C-enriched CO$_2$ (0.75 bar at RT): (A) ^{13}C MAS NMR spectrum; (B) 2D ^{1}H–^{13}C HETCOR MAS NMR spectra collected at room temperature and at two distinct contact times (ct). The host–CO$_2$ cross peaks are highlighted in red. Chemical structures of TBS and DAB with labels (below). (C) Electrostatic potential projected on CO$_2$ molecules by the DAB and TBS host moieties. The CO$_2$ molecules were localized by DFT calculations.

pressures (<0.1 bar) and 110 at 1 bar. The CO_2/N_2 selectivity at room temperature was 540, as calculated using the ratio of Henry's constants (ESI†). This is one of the highest selectivities shown to date in porous molecular materials.[19,20,24,47]

Furthermore, the isosteric heat of adsorption calculated for methane is 21.0 kJ mol^{-1}, which is remarkably high compared to those of typical 3D frameworks with open metal sites or higher surface areas (Fig. 2C).[9] It is comparable to SOF-1 ($\Delta H = 20.8$ kJ mol^{-1}) and one of the highest reported values in microporous polymers and crystals.[23,51–53]

Screwing dynamics and diffusion rate of CO_2 in the channels

The remarkable CO_2-matrix association allowed direct observation of the gas exploring the nanochannels by NMR spectroscopy. The ^{13}C MAS NMR spectrum showed two dominant signals at $\delta_c = 125.5$ and 125.8 ppm for ^{13}C-enriched CO_2: the former identifying free CO_2 and the latter CO_2 housed in the confined space of the crystal (Fig. 3A). The downfield signal is generated by the magnetic susceptibility effect experienced by CO_2 molecules embedded in the polar environment of the crystal. In the cross-polarization (CP) spectrum, the $\delta_c = 125.8$ ppm signal is largely dominating, for the fast magnetization transfer even at room temperature, from the matrix hydrogens to the CO_2 carbons lying a short distance away (<1 nm),[54] proving that the gas is exceptionally well-retained (ESI†). This is a remarkable result given the well-known difficulty of transferring nuclear polarization in conventional systems from a solid towards a gas, because of the short gas residence time, especially at room temperature.

The surprising efficiency of gas–solid CP was exploited for the success of 2D ^1H–^{13}C CP NMR, which allowed for both *in situ* spectroscopic detection of CO_2 and the identification of the specific interaction sites (Fig. 3B).[33,55,56] Even at a contact time as short as 0.5 ms and room temperature, CO_2 carbon nuclei receive magnetization from the amidinium hydrogens (at $\delta_H = 7.4$ ppm), showing the short distances of the gas from these

Fig. 4 (A) Variable temperature ^{13}C NMR spectra of the CPOS-5/$^{13}CO_2$ sample under static conditions. The chemical shift anisotropic lineshape of solid CO_2, simulated starting from the main tensor components, is reported below for comparison. (B) Inclination angle (θ) of the CO_2 main-axis with respect to the reorientation-axis z about which the 90° (ϕ angle) jump occurs. (C) Screwing mechanism for CO_2 rototranslational dynamics in the channel: the 90° rotation angle of CO_2 projection onto the *ab*-plane and along the channel *c*-axis for CO_2 reorientation from one site to the next. (D) Overlay of the CO_2 positions along the channel as calculated by the DFT transition state method. (E) Helical trajectory of one CO_2 oxygen atom (red spheres) about the channel axis (blue bar). (F) Arrhenius plot of reorientational rates (*k*) *versus* the inverse of temperature. (G) Calculated energy profile for the rototranslation of CO_2 along the channel.

species lining the channel walls. The short internuclear distances were confirmed by *ab initio* DFT calculations, which pointed out the CO_2 location and a distance of 3.24 Å between the N–H hydrogen and CO_2 carbon. The close proximity of the CO_2 carbon with the N–H group is imposed by the interaction of one of the CO_2 oxygens with the amidinium cation. Also the aromatic C–H group of DAB undergoes favorable interactions with CO_2 oxygens as demonstrated by the highly positive electrostatic potentials (Fig. 3C: the red regions on the oxygen atom of CO_2). Actually, at a longer contact time of 1 ms the 2D NMR spectrum highlights the correlation between the aromatic C–H of DAB and CO_2 carbon (distance of 4.18 Å). With regard to the organosulfonate anions, DFT calculations show CO_2 molecules clamped in between the oxygens of two TBS sulfonate groups (Fig. 3C: the blue regions on the carbon atom of CO_2), keeping the C–H hydrogens of TBS far apart from the CO_2 carbon (distance of 5.75 Å), consistent with the absence of NMR cross-correlations. From the combined NMR and modelling approach, we can conclude that the charge distribution of the host complements the charges on the CO_2 molecule and determines the stabilization of the gas in the channels.

Remarkably, multiple aspects of the dynamics of the CO_2 molecules in the channels came to light from variable temperature ^{13}C NMR spectra recorded in the static mode (Fig. 4A). Actually, the spectra depicted axial chemical shift anisotropy (CSA) restricted to a fraction of the total spectral width of solid CO_2 in the bulk.[57,58] From the NMR lineshape simulation we were able to determine the mechanism of motion, the dynamics and the inclination of CO_2 molecules in the channels. The lineshape at room temperature describes a rapid 4-site re-orientation of CO_2 molecules by a 90° jump mechanism (Fig. 4B). Nonetheless, the CO_2 main axis maintains an inclination angle equal to $\theta = 56.7°$ with respect to the rotation axis. By lowering the temperature to 215 K, the inclination increases to 58.1° due to the increased loading and the larger contribution of CO_2–CO_2 interactions (ESI†). Notably, by the spectral analysis at variable temperature, it was possible to measure the 90° jump rates (k) that are higher than 10^6 Hz at room temperature and still over 10^5 Hz at 215 K.

To understand in-depth the NMR determinations of the gas diffusing in the tight-fitting channels, molecular dynamics combined with *ab initio* calculations provided a model for the energy profile and interaction sites perceived by CO_2 travelling in the channels. Each site accommodates a CO_2 molecule at a time and imparts to the CO_2 molecule an average inclination angle θ of 57°–58°, in perfect agreement ($\pm 0.7°$) with the NMR data (ESI†). Regarding the fast 90° re-orientation, it cannot occur within the same site without a very high energy cost, for steric and electrostatic reasons. In contrast, the next site along the channel (symmetry related by a four-fold screw axis, 4_1) can host CO_2 after its 90° turn (Fig. 4C). Thus, CO_2 reorientation, observed by NMR, implies rotation correlated with sliding motion to the next site with the rate of 10^6 steps per second (Fig. 4D). Indeed, the unique feature of this diffusion phenomenon is the concerted roto-translation mechanism (*i.e.* simultaneous rotation and translation along the c axis) occurring with extremely rapid dynamics of the confined CO_2, which follows a helical trajectory by a screwing path along a single file (Fig. 4E). From the NMR jump

rates (k) *vs.* temperature, an Arrhenius plot can be derived, establishing a small activation energy of 2.9 kcal mol^{-1} (Fig. 4F), in excellent agreement with the energy barrier of 2.1 kcal mol^{-1} for a diffusion step of CO_2 molecules, during the helical transport, as calculated by DFT analysis (Fig. 4G).

Conclusions

Multifunctional tetra-anionic and di-cationic molecules combine together to form frameworks with the property of being permanently porous. The crystalline framework was designed by the use of intrinsically rigid molecules as constructive elements and ionic interactions between sulfonate anions and amidinium cations. The ionic patterning of the crystalline channels allows the establishment of high interactions of 35 kJ mol^{-1}, ideal for CO_2 capture/release cycles. This high energy value stably retains the quadrupolar molecules of CO_2. Such CO_2 sequestration was so efficient that the CO_2/N_2 selectivity values at low pressures (<0.1 bar) range from 320 to 690.

The interaction strength of the CO_2 with the host was recognized by the striking capability of CO_2 to receive nuclear polarization from the framework at room temperature and to develop the anisotropic patterns in the static ^{13}C NMR spectra. A unique screwing mechanism of CO_2, which follows the helical track of the charges on the channel walls, was observed. The rate of a single step (>10^6 steps per second) in the diffusion trajectory along the tunnel could be unconventionally established by NMR. The orientational and dynamical features are enforced by the computational models of gas–framework interactions. The contribution of the charges patterning the channel walls is of paramount importance for directing the association of a gas, such as CO_2, with the host. These pieces of evidence encourage the use of multiple charge molecules of opposite polarity to spontaneously self-organize into functional materials endowed with high thermal stability and exploit the rich modularity of polyanions and polycations to design structures tailored to a specific gas for capture and sequestration.

Moreover, the fabrication of artificial charged channels in crystalline materials with a high degree of order and uniformity as well as a controllable structure promotes the understanding of the role of electrostatic interactions in the transport properties of transmembrane channels of biological systems.[45,59] Indeed, the CO_2 diffusion in helical narrow channels, such as in aquaporins, plays a strategic role in the selection and concentration of gases in plant cells.[59] Our newly fabricated crystalline channels share helical and sub-nanometric structural features, and transport properties in a single file through the polar environment, thus achieving high selectivity.

Conflicts of interest

There are no conflicts to declare.

Acknowledgements

Notes and references

1 S. Kitagawa, R. Kitaura and S.-I. Noro, Functional Porous Coordination Polymers, *Angew. Chem., Int. Ed.*, 2004, **43**, 2334–2375.

2 A. Schoedel, Z. Li and O. M. Yaghi, The role of metal–organic frameworks in a carbon-neutral energy cycle, *Nat. Energy*, 2016, **1**, 1–13.

3 H. C. Zhou and S. Kitagawa, Metal–Organic Frameworks (MOFs), *Chem. Soc. Rev.*, 2014, **43**, 5415–5418.

4 S. Das, P. Heasman, T. Ben and S. Qiu, Porous Organic Materials, *Chem. Rev.*, 2017, **117**, 1515–1563.

5 Z. Zhang and M. J. Zaworotko, Template-directed synthesis of metal–organic materials, *Chem. Soc. Rev.*, 2014, **43**, 5444–5445.

6 A. Thomas, Functional Materials: From Hard to Soft Porous Frameworks, *Angew. Chem., Int. Ed.*, 2010, **49**, 8328–8344.

7 P. Ramaswamy, N. E. Wong and G. H. K. Shimizu, MOFs as proton conductors – challenges and opportunities, *Chem. Soc. Rev.*, 2014, **43**, 5913–5932.

8 M. Simard, D. Su and J. D. Wuest, Use of hydrogen bonds to control molecular aggregation. Self-assembly of three-dimensional networks with large chambers, *J. Am. Chem. Soc.*, 1991, **113**, 4696–4698.

9 G. Zhang and M. Mastalerz, Organic cage compounds – From shape-persistency to function, *Chem. Soc. Rev.*, 2014, **43**, 1934–1947.

10 T. Hasell and A. I. Cooper, Porous organic cages: soluble, modular and molecular pores, *Nat. Rev. Mater.*, 2016, **1**, 1–14.

11 N. B. J. McKeown, Nanoporous molecular crystals, *J. Mater. Chem.*, 2010, **20**, 10588–10597.

12 A. G. Skaterand and A. I. Cooper, Porous materials. Function-led design of new porous materials, *Science*, 2015, **348**, aaa8075.

13 P. Sozzani, S. Bracco, A. Comotti, L. Ferrettia and R. Simonutti, Methane and carbon dioxide storage in a porous van der Waals crystal, *Angew. Chem., Int. Ed.*, 2005, **44**, 1816–1820.

14 L. J. Barbour, Crystal porosity and the burden of proof, *Chem. Commun.*, 2006, 1163–1168.

15 K. J. Msayib, D. Book, P. M. Budd, N. Chaukura, K. D. M. Harris, M. Helliwell, S. Tedds, A. Walton, J. E. Warren, M. Xu and N. B. McKeown, Nitrogen and Hydrogen Adsorption by an Organic Microporous Crystal, *Angew. Chem., Int. Ed.*, 2009, **48**, 3273–3277.

16 A. Comotti, S. Bracco, G. Distefano and P. Sozzani, Methane, carbon dioxide and hydrogen storage in nanoporous dipeptide-based materials, *Chem. Commun.*, 2009, 284–286.

17 H. Kim, H. Kim, Y. Kim, M. Yoon, S. Lim, S. M. Park, G. Seo and K. Kim, Highly Selective Carbon Dioxide Sorption in an Organic Molecular Porous Material, *J. Am. Chem. Soc.*, 2010, **132**, 12200–12202.

18 M. Mastalerz, M. W. Schneider, I. M. Oppel and O. Presly, A Salicylbisimine Cage Compound with High Surface Area and Selective CO_2/CH_4 Adsorption, *Angew. Chem., Int. Ed.*, 2011, **50**, 1046–1051.

19 V. N. Yadav, A. Comotti, P. Sozzani, S. Bracco, T. Bonge-Hansen, M. Hennum and C. H. Gorbitz, Microporous Molecular Materials from Dipeptides Containing Non-proteinogenic Residues, *Angew. Chem., Int. Ed.*, 2015, **54**, 15684–15688.

20 I. Bassanetti, S. Bracco, A. Comotti, M. Negroni, C. Bezuidenhout, S. Canossa, P. P. Mazzeo, L. Marchio' and P. Sozzani, Flexible porous molecular materials responsive to CO_2, CH_4 and Xe stimuli, *J. Mater. Chem. A*, 2018, **6**, 14231–14239.

21 M. Baroncini, S. D'Agostino, G. Bergamini, P. Ceroni, A. Comotti, P. Sozzani, I. Bassanetti, F. Grepioni, T. M. Hernandez, S. Silvi, M. Venturi and A. Credi, Photoinduced reversible switching of porosity in molecular crystals based on star-shaped azobenzene tetramers, *Nat. Chem.*, 2015, **7**, 634–640.

22 Y. He, S. Xiang and B. Chen, A Microporous Hydrogen-Bonded Organic Framework for Highly Selective C_2H_2/C_2H_4 Separation at Ambient Temperature, *J. Am. Chem. Soc.*, 2011, **133**, 14570–14573.

23 W. Yang, *et al.*, Exceptional Thermal Stability in a Supramolecular Organic Framework: Porosity and Gas Storage, *J. Am. Chem. Soc.*, 2010, **132**, 14457–14469.

24 H. Wang, *et al.*, A Flexible Microporous Hydrogen-Bonded Organic Framework for Gas Sorption and Separation, *J. Am. Chem. Soc.*, 2015, **137**, 9963–9970.

25 W. Yan, *et al.*, A triptycene-based porous hydrogen-bonded organic framework for guest incorporation with tailored fitting, *Chem. Commun.*, 2017, **53**, 3677–3680.

26 C. A. Zentner, H. W. H. Lai, J. T. Greenfield, R. A. Wiscons, M. Zeller, C. F. Campana, O. Talu, S. A. FitzGeralde and J. L. C. Rowsel, High surface area and Z' in a thermally stable 8-fold polycatenated hydrogen-bonded framework, *Chem. Commun.*, 2015, **51**, 11642–11645.

27 P. Li, *et al.*, A rod-packing microporous hydrogen-bonded organic framework for highly selective separation of C_2H_2/CO_2 at room temperature, *Angew. Chem., Int. Ed.*, 2015, **54**, 574–577.

28 F. Hu, *et al.*, An Ultrastable and Easily Regenerated Hydrogen-Bonded Organic Molecular Framework with Permanent Porosity, *Angew. Chem., Int. Ed.*, 2017, **56**, 2101–2104.

29 I. Hisaki, S. Nakagawa, N. Tohnai and M. Miyata, A C_3-Symmetric Macrocycle Based, Hydrogen Bonded, Multiporous Hexagonal Network as a Motif of Porous Molecular Crystals, *Angew. Chem., Int. Ed.*, 2015, **54**, 3008–3012.

30 T. Adachi and M. D. Ward, Versatile and Resilient Hydrogen-Bonded Host Frameworks, *Acc. Chem. Res.*, 2016, **49**, 2669–2679.

31 Y. Liu, C. Hu, A. Comotti and M. D. Ward, Supramolecular Archimedean cages assembled with 72 hydrogen bonds, *Science*, 2011, **333**, 436–440.

32 A. Comotti, S. Bracco, A. Yamamoto, M. Beretta, T. Hirukawa, N. Tohnai, M. Miyata and P. Sozzani,

Engineering Switchable Rotors in Molecular Crystals with Open Porosity, *J. Am. Chem. Soc.*, 2014, **136**, 618–621.

33 S. Bracco, T. Miyano, M. Negroni, I. Bassanetti, L. Marchio', P. Sozzani, N. Tohnai and A. Comotti, CO_2 regulates molecular rotor dynamics in porous materials, *Chem. Commun.*, 2017, **53**, 7776–7779.

34 G. Xing, I. Bassanetti, T. Ben, S. Bracco, P. Sozzani, L. Marchio' and A. Comotti, Multifunctional Organosulfonate Anions Self-Assembled with Organic Cations by Charge-Assisted Hydrogen Bonds and the Cooperation of Water, *Cryst. Growth Des.*, 2018, **18**, 2082–2092.

35 G. Xing, T. Yan, S. Das, T. Bena and S. Qiu, Synthesis of Crystalline Porous Organic Salts with High Proton Conductivity, *Angew. Chem., Int. Ed.*, 2018, **57**, 5345–5349.

36 X. Wang, M. Simard and J. Wuest, Molecular Tectonics. Three-Dimensional Organic Networks with Zeolitic Properties, *J. Am. Chem. Soc.*, 1994, **116**, 12119–12120.

37 M. J. Zaworotko, Crystal engineering of diamondoid networks, *Chem. Soc. Rev.*, 1994, **23**, 283–288.

38 T. Ben, H. Ren, S. Ma, D. Cao, J. Lan, X. Jing, W. Wang, J. Xu, F. Deng, J. M. Simmons, S. Qui and G. Zhu, Targeted synthesis of a porous aromatic framework with high stability and exceptionally high surface area, *Angew. Chem., Int. Ed.*, 2009, **48**, 9457–9460.

39 W. Lu, D. Yuan, D. Zhao, C. I. Schilling, O. Plietzsch, T. Muller, S. Bräse, J. Guenther, J. Blümel, R. Krishna, Z. Li and H.-C. Zhou, Porous Polymer Networks: Synthesis, Porosity, and Applications in Gas Storage/Separation, *Chem. Mater.*, 2010, **22**, 5964–5972.

40 W. Lu, D. Yuan, J. Sculley, D. Zhao, R. Krishna and H.-C. Zhou, Sulfonate-Grafted Porous Polymer Networks for Preferential CO_2 Adsorption at Low Pressure, *J. Am. Chem. Soc.*, 2011, **133**, 18126–18129.

41 P. Pandey, O. K. Farha, A. M. Spokoyny, C. A. Mirkin, M. G. Kanatzidis, J. T. Hupp and S. T. Nguyen, A "click-based" porous organic polymer from tetrahedral building blocks, *J. Mater. Chem.*, 2011, **21**, 1700–1703.

42 S. S. Han, H. Furukawa, O. M. Yaghia and W. A. Goddard, Covalent Organic Frameworks as Exceptional Hydrogen Storage Materials, *J. Am. Chem. Soc.*, 2008, **130**, 11580–11581.

43 H. Furukawa and O. M. Yaghi, Storage of Hydrogen, Methane, and Carbon Dioxide in Highly Porous Covalent Organic Frameworks for Clean Energy Applications, *J. Am. Chem. Soc.*, 2009, **131**, 8875–8883.

44 A. Comotti, J. Perego, D. Piga, S. Bracco and P. Sozzani, Expandable porous organic frameworks with built-in amino and hydroxyl functions for CO_2 and CH_4 capture, *Chem. Commun.*, 2018, **54**, 9321–9324.

45 R. E. Hibbs and E. Gouaux, Principles of activation and permeation in an anion-selective Cys-loop receptor, *Nature*, 2011, **474**, 54–60.

46 A. O. Yazaydin, R. Snurr, T.-H. Park, K. Koh, J. Liu, M. D. LeVan, A. I. Benin, P. Jakubczak, M. Lanuza, D. B. Galloway, J. J. Low and R. R. Willis, Screening of Metal–Organic Frameworks for Carbon Dioxide Capture from Flue Gas Using a Combined Experimental and Modeling Approach, *J. Am. Chem. Soc.*, 2009, **131**, 18198–18199.

47 J. Lu, C. P. Krap, M. Suyetin, N. H. Alsmail, Y. Yan, S. Yang, W. Lewis, E. Bichoutskaia, C. C. Tang, A. J. Blake, R. Cao and M. Schoeder, A Robust Binary Supramolecular Organic Framework (SOF) with High CO_2 Adsorption and Selectivity, *J. Am. Chem. Soc.*, 2014, **136**, 12828–12831.

48 S. Bourrelly, P. L. Llewellyn, C. Serre, F. Millange, T. Loiseau and G. Férey, Different Adsorption Behaviors of Methane and Carbon Dioxide in the Isotypic Nanoporous Metal Terephthalates MIL-53 and MIL-47, *J. Am. Chem. Soc.*, 2005, **127**, 13519–13521.

49 P. L. Llewellyn, S. Bourrelly, C. Serre, A. Vimont, M. Daturi, L. Hamon, G. De Weireld, J.-S. Chang, D.-Y. Hong, Y.-K. Hwang, S.-H. Jhung and G. Férey, High Uptakes of CO_2 and CH_4 in Mesoporous Metal–Organic Frameworks MIL-100 and MIL-101, *Langmuir*, 2008, **24**, 7245–7250.

50 J.-S. Lee, J.-H. Kim, J.-T. Kim, J.-K. Suh, J.-M. Lee and C.-H. Lee, Adsorption Equilibria of CO_2 on Zeolite 13X and Zeolite X/Activated Carbon Composite, *J. Chem. Eng. Data*, 2002, **47**, 1237–1242.

51 B. Li, H.-M. Wen, W. Zhou, Q. Xu and B. Chen, Porous Metal–Organic Frameworks: Promising Materials for Methane Storage, *Chem*, 2016, **1**, 557–580.

52 J. A. Mason, M. Veenstra and J. R. Long, Evaluating metal–organic frameworks for natural gas storage, *Chem. Sci.*, 2014, **5**, 32–51.

53 H. Li, K. Wang, Y. Sun, C. T. Lollar, J. Li and H.-C. Zhou, Recent advances in gas storage and separation using metal–organic frameworks, *Mater. Today*, 2018, **21**, 108–121.

54 A. Pines, J. S. Gibby and J. S. Waugh, Proton-enhanced NMR of dilute spins in solids, *J. Chem. Phys.*, 1973, **59**, 569–590.

55 I. Bassanetti, A. Comotti, P. Sozzani, S. Bracco, G. Calestani, F. Mezzadri and L. Marchiò, Porous Molecular Crystals by Macrocyclic Coordination Supramolecules, *J. Am. Chem. Soc.*, 2014, **136**, 14883–14895.

56 A. Comotti, A. Fraccarollo, S. Bracco, M. Beretta, G. Distefano, M. Cossi, L. Marchese, C. Riccardi and P. Sozzani, Porous dipeptide crystals as selective CO_2 adsorbents: experimental isotherms *vs.* grand canonical Monte Carlo simulations and MAS NMR spectroscopy, *CrystEngComm*, 2013, **15**, 1503–1507.

57 C. R. Bowers, H. W. Long, T. Pietrass, H. C. Gaede and A. Pines, A. Cross polarization from laser-polarized solid xenon to $^{13}CO_2$ by low-field thermal mixing, *Chem. Phys. Lett.*, 1993, **205**, 168–170.

58 X. Kong, E. Scott, W. Ding, J. A. Mason, J. R. Long and A. A. Reimer, CO_2 Dynamics in a Metal–Organic Framework with Open Metal Sites, *J. Am. Chem. Soc.*, 2012, **134**, 14341–14344.

59 N. Uehlein, C. Lovisolo, F. Siefritz and R. Kaldenhoff, The tobacco aquaporin NtAQP1 is a membrane CO_2 pore with physiological functions, *Nature*, 2003, **425**, 734–737.